Results in Physics 44 (2023) 106158

Contents lists available at ScienceDirect

Results in Physics

journal homepage: www.elsevier.com/locate/rinp

Importance of core and shell sizes in the localization of the electron and hole in the formation of type I or type II excitons in spherical *CdSe/ZnTe* and *CdSe/CdTe* quantum dots.

N. Aghoutane [a,*], L.M. Pérez [b], D. Laroze [a], M. El-Yadri [c], E. Feddi [c,d]

[a] Instituto de Alta Investigación, CEDENNA, Universidad de Tarapacá, Casilla 7D, Arica, Chile
[b] Departamento de Física, FACI, Universidad de Tarapacá, Casilla 7D, Arica, Chile
[c] Group of Optoelectronic of Semiconductors and Nanomaterials, ENSAM, Mohammed V University in Rabat, Morocco
[d] Institute of Applied Physics, Mohammed VI Polytechnic University, Lot 660, Hay Moulay Rachid Ben Guerir, 43150, Morocco

ARTICLE INFO

Keywords:
Type II core/shell
Exciton
Critical radius
Effective optical band gap
Binding energy

ABSTRACT

Semiconductor core/shell quantum dots represent a promising class of nanostructure that can provide new techniques of control for performing the electronic and optical properties. Through each combination formed by the core and the shell radii and the confinement effect, the trapped charge carries behave differently, which obviously has a direct effect on the semiconductor properties. Studying the behavior of charge carriers is one of the most important steps in understanding the semiconductor performance when it undergoes certain conditions, which inevitably can offer other benefits for various applications. The electron and hole localizations strongly depend on core and shell sizes, but determining these limit sizes has not been sufficiently discussed in the literature. This paper gives a detailed theoretical study describing the three cases of electron and hole positions in two different type II core/shell quantum dots, CdSe/ZnTe and CdSe/CdTe considering the core and shell sizes. Our numerical calculations show that two significant critical radii of the core allow to switch between the exciton type I and type II quasi-particle. As a function of the shell thickness, the ground state energy of the electron is found to be higher when the core radius is small; contrariwise, the hole ground state energy remains smaller. Afterward, these specific variations influence the ground state binding energy of the correlated electron–hole quasi-particle (exciton), leading to a particular behavior of this energy as a function of the core and shell sizes.

Introduction

The development of nanostructures (NS) research has considerably advanced since the first synthesis of nanocrystals [1]. Over the last two decades, we have moved from controlling sizes to shapes [2–4]. These nanostructures attract great interest thanks to their similar behavior to the atom, i.e., quantifying electronic states with a finite number of confined particles and the possibility of artificially controlling their behavior through modifying dimensions and shapes. Because of modern techniques in synthesizing semiconductors materials, new architectural structures can be obtained known as core/shell NS. An exterior shell can cover an inner material that makes up the core with a different band gap. These structures provide new and exciting optical and electronic properties due to the reinforcement of orbitals overlap between confined charge carriers. Depending on the band alignments, the core/shell syntheses were classified into three types. Type I [5] (the particles are localized in the core), inverted type I [6] (the particles are confined in the shell), and type II (one of the charge carriers is confined in the core and the other in the shell) [7]. By controlling the shell thickness or core size, type II can be highly recommended by looking at the change that can be made in the energy levels of the electron, hole, and exciton [8–10]. Their fascinating properties attract significant interest in the nanostructures research community, which manifests in a wide variety of applications such as light-emitting-diodes, inter-band lasers, wavelength detectors, and photovoltaics [11–17]. Several investigations have been devoted to type II NS experimentally [18–31] and theoretically [32–38]. It has been demonstrated that the energy of the particles (electron, hole, exciton...) depends directly on the size of a core/shell type II. The binding energy of biexciton confined in type II heteronanomaterial has been reported theoretically by Piryatinski et al. [7]. Their results show a strong effect of quantum confinement and dielectric mismatch on exciton–exciton repulsion. P.G. McDonald

* Corresponding author.
E-mail address: noreddine.aghoutane@gmail.com (N. Aghoutane).

https://doi.org/10.1016/j.rinp.2022.106158
Received 15 September 2022; Received in revised form 17 November 2022; Accepted 3 December 2022
Available online 5 December 2022

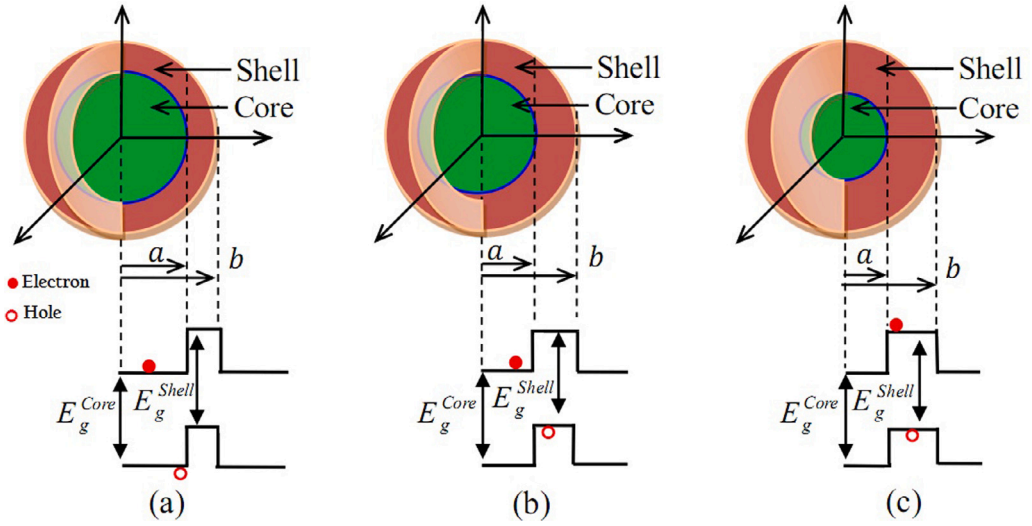

Fig. 1. Pictorial view of type II core/shell nanostructure: for a fixed shell size, one can distinguish different particle localization regimes according to core radius: (a) corresponds to core radius $a > a_e^c$ and $a > a_h^c$ which means that the electron energy $E_e < V_e$ and hole energy $E_h > V_h$, electron and hole are localized within core, (b) corresponds to the case: $a > a_e^c$ and $a < a_h^c$, $E_i < V_i$ (i=e,h), electron is localized within core while hole escapes to the shell and (c) corresponds to core radius $a < a_e^c$ and $a < a_h^c$, $E_e > V_e$ and $E_h < V_h$, where the electron and hole are localized within shell region.

et al. [39] have investigated the shell thickness effect on the electron–hole interaction energies and the exciton–exciton confined in core/shell quantum dots type I and type II. Their calculation shows a decrease in the correlated energy of the exciton by increasing the shell thickness for a fixed core radius. S.N. Saravanamoorthy et al. have examined the pressure effect on the optical and electronic properties of excitons localized in Type II core/shell [40]. Other studies have treated the size effect on the electronic and optical properties of type II *CdSe/ZnTe* and *CdSe/CdTe* core/shell quantum dot. These studies have shown that the electronic and optical properties are deeply dependent on the size of the materials [41–44].

Looking closely at all these studies, we notice that they need to consider critical radius, which is a significant factor in determining the charge carriers' positions when the core and shell radii vary. In this paper, we will present a general study that considers all the possibilities of the existence of the electron (e) and the hole (h), whether inside the core or in the shell. Therefore, to investigate the behaviors of the electron and hole ground state energies in type II spherical NS for *CdSe/ZnTe* and *CdSe/CdTe* materials by considering the effect of inner (core) and outer (shell) radii on the localization of charge carriers, we determine the critical radii corresponding to electron and hole dislocation through *CdSe/ZnTe* and *CdSe/CdTe*, respectively. Following this, this study will be extended to the influence of the Coulomb interaction and the core/shell sizes on the correlated (e–h) pair (exciton). The calculations were performed within the framework of effective mass approximation by choosing adequate wave functions considering the correlations between the particles. The structure of our article begins with our theoretical model used in this study, and then we discuss the results obtained for the correlated and uncorrelated pair energies (e, h); finally, the study wraps up with a conclusion.

Background theory

In this study, we consider a quantum dot (QD) NS composed of a spherical core material with a dielectric constant ε_1 and radius a overcoated by another spherical shell material with radius b and dielectric constant ε_2. For the core/shell QD type II system, which constitutes our issue, we have to choose specific materials to meet our objectives. In this work, we consider two different core/shell compounds each other: *CdSe/ZnTe* and *CdSe/CdTe*. The choice of these two materials is due to (i) the possibility of their synthesis and (ii) the convergence of their dielectric constants, which allows the solution of the Schrödinger

Table 1
Radial wave functions $R_{n,l}^i(r_i)$ and energy-relations k_i for different regions of the electron and hole localization.

	$R_{n,l}^e(r_e)$	$R_{n,l}^h(r_h)$
bound states $E_i < V_i$	$\begin{cases} A_{1e}\frac{\sin(k_{1e}r_e)}{r_e} & \text{if } 0 < r_e < a \\ A_{2e}\frac{\sinh(k_{2e}(r_e-b))}{r_e} & \text{if } a < r_e < b \end{cases}$ with : $k_{1e} = \sqrt{\frac{2m_{1e}^* E_e}{\hbar^2}}$, $k_{1e} = \sqrt{\frac{2m_{2e}^*(V_e-E_e)}{\hbar^2}}$	$\begin{cases} A_{1h}\frac{\sinh(k_{1h}r_h)}{r_h} & \text{if } 0 < r_h < a \\ A_{3h}\frac{\sin(k_{3h}(r_h-b))}{r_h} & \text{if } a < r_h < b \end{cases}$ with : $k_{1h} = \sqrt{\frac{2m_{1h}^*(V_h-E_h)}{\hbar^2}}$, $k_{3h} = \sqrt{\frac{2m_{2h}^* E_h}{\hbar^2}}$
unbound states $E_i > V_i$	$\begin{cases} A_{1e}\frac{\sin(k_{1e}r_e)}{r_e} & \text{if } 0 < r_e < a \\ A_{3e}\frac{\sin(k_{3e}(r_e-b))}{r_e} & \text{if } a < r_e < b \end{cases}$ with : $k_{1e} = \sqrt{\frac{2m_{1e}^* E_e}{\hbar^2}}$, $k_{3e} = \sqrt{\frac{2m_{2e}^*(E_e-V_e)}{\hbar^2}}$	$\begin{cases} A_{2h}\frac{\sin(k_{2h}r_h)}{r_h} & \text{if } 0 < r_h < a \\ A_{3h}\frac{\sin(k_{3h}(r_h-b))}{r_h} & \text{if } a < r_h < b \end{cases}$ with : $k_{2h} = \sqrt{\frac{2m_{1h}^*(E_h-V_h)}{\hbar^2}}$, $k_{3h} = \sqrt{\frac{2m_{2h}^* E_h}{\hbar^2}}$

equation without the dielectric mismatch but only with the direct Coulomb interaction between the particles (electron and hole). For one particle, the Hamiltonian can be written as:

$$H_i = -\frac{\hbar^2}{2m_i^*(r_i)}\Delta_i + V_i(r_i),\ (i = e, h) \tag{1}$$

The first term is the kinetic energy operator; r_i and m_i^* are the radius and the effective mass of the particle i *(i=e,h)*, respectively. Because of the discontinuity of the core/shell structure, electron and hole masses in different regions are related to their positions in both materials by the relation:

$$m_i^*(r_i) = \begin{cases} m_{1i}^* & \text{for} \quad 0 < r_i < a \\ m_{2i}^* & \text{for} \quad a < r_i < b \end{cases} \tag{2}$$

The second term V_i denotes the electron and hole confinement potentials. They take the following forms:

$$V_e = \begin{cases} 0, & \text{for} \quad 0 < r_e < a \\ V_{0e}, & \text{for} \quad a < r_e < b \\ \infty & otherwise \end{cases} \tag{3}$$

$$V_h = \begin{cases} V_{0h}, & \text{for} \quad 0 < r_h < a \\ 0, & \text{for} \quad a < r_h < b \\ \infty & otherwise \end{cases} \tag{4}$$

To obtain the wave eigenfunctions of the electron and hole, it is necessary to solve the Schrödinger equation:

$$H_i\psi_i(r_i) = E_i\psi_i(r_i)$$

The resolution of this equation in spherical coordinates (r, θ, φ) gives:

$$\psi_i\left(r_i\right) = R^i_{n,l}\left(r_i\right) Y^i_{l,m}(\theta,\ \varphi), \quad i = e,\ h$$

Where $Y^i_{l,m}(\theta, \varphi)$ is a spherical harmonics functions, n, l and m are respectively the principal, orbital and magnetic quantum numbers. The ground state of the particles is corresponding to $n = 1,\ l = 0$ and $m = 0$. To understand the behavior of the electron and hole particles under the finite band offsets model, we should include the critical radius concept. Indeed, the electron (hole) can move from the core (shell) region to the shell (core) region when the core radius reaches critical values a^c_i for a given shell radius b. These values can be obtained numerically when the energy of the particles (e, h) is equal to the band offsets ($E_i = V_i$). We recall that two cases are possible for each particle: (i) a bound state ($E_i < V_i$) and (ii) an unbound state ($E_i > V_i$). Determining the electronic states of the particles in this structure requires the resolution of the Schrödinger equation in all possible positions of both particles. Table 1 shows the explicit expressions of the radial parts of the ground state wave functions and the energies corresponding to both cases. From these expressions, we can build the exciton trial wave functions considering the localization of the electron and the hole simultaneously (configuration a, b, and c in Fig. 1).

The continuity of the radial wave function at $r_i = a$ gives the transcendental equation for computing the ground (bound and unbound) states energy E_i:

$$\begin{cases} \psi_i\,(core)\big|_{r_i=a} = \psi_i\,(shell)\big|_{r_i=a} \\ \frac{1}{m^*_{1i}}\frac{d\ \psi_i(core)}{dr_i}\Big|_{r_i=a} = \frac{1}{m^*_{2i}}\frac{d\ \psi_i(shell)}{dr_i}\Big|_{r_i=a} \end{cases} \quad i = e,\ h \tag{5}$$

Note that when $E_i = V_i$, the previous equations coincide and lead to significant expressions. From these expressions, we can conclude the critical core radius a^c_i, from which the particles i leave the core (shell) material.

For electron:

$$\frac{m^*_{2e}}{m^*_{1e}}\left(a^c_e\sqrt{\frac{2m^*_{1e}V_e}{\hbar^2}}\ cot\left(\sqrt{\frac{2m^*_{1e}V_e}{\hbar^2}}\ a^c_e\right) - 1\right) = \left(\frac{b}{\left(a^c_e - b\right)}\right) \tag{6}$$

and for hole:

$$1 - \left(a^c_h\sqrt{\frac{2m^*_{2h}V_h}{\hbar^2}}\ cot\left(\sqrt{\frac{2m^*_{2h}V_h}{\hbar^2}}\ (a^c_h - b)\right)\right) = 0 \tag{7}$$

The electron and hole can be correlated to form the known exciton (X). For this reason, the next part will be devoted to determining the exciton ground states confined in the considered structure. The Hamiltonian of exciton within this structure can be written as:

$$H_X = -\frac{\hbar^2}{2m^*_{ie}\left(r_e\right)}\Delta_e - \frac{\hbar^2}{2m^*_{ih}\left(r_h\right)}\Delta_h + V_e + V_h - \frac{e^2}{\varepsilon(r_e,\ r_h)\left|r_e - r_h\right|} \tag{8}$$

The first and second terms describe the kinetic energies of the electron and hole, respectively. V_e and V_h are the confining potentials. The last term is the Coulomb interaction.

In our model, we use as a unit of energy the excitonic effective Rydberg $R_X = \frac{\hbar^2}{2\tilde{\mu}\tilde{a}_x^2}$. As the unit of length, the exciton effective Bohr radius $\tilde{a}_x = \frac{\tilde{\varepsilon}\hbar^2}{e^2\tilde{\mu}}$, with $(\tilde{\mu})^{-1} = (\tilde{m}^*_e)^{-1} + (\tilde{m}^*_h)^{-1}$ is the reduced mass of exciton, $\tilde{m}^*_i = \sqrt{m^*_{i1}m^*_{i2}}$ is the single particle (i) mean effective mass, and $\tilde{\varepsilon} = \sqrt{\varepsilon_1\varepsilon_2}$ is the mean relative dielectric constant. By using these reduced units, the Hamiltonian of the system becomes:

$$H_X = -\frac{\tilde{\mu}}{m^*_{ie}\left(r_e\right)}\Delta_e - \frac{\tilde{\mu}}{m^*_{ih}\left(r_h\right)}\Delta_h + V_e + V_h - \frac{2\tilde{\varepsilon}}{\varepsilon(r_e,\ r_h)r_{eh}} \tag{9}$$

Table 2
Physical parameters of the studied materials.

	CdSe [47]	CdTe [34]	ZnTe [47]
E_g(eV)	1.75	1.61	2.2
ε	10.6	10.4	9.7
m^*_e/m_0	0.13	0.096	0.15
m^*_h/m_0	0.4	0.4	0.2

with

$$\Delta_e = \frac{\partial^2}{\partial r_e^2} + \frac{2}{r_e}\frac{\partial}{\partial r_e} + \left(\frac{r_e^2 - r_h^2 + r_{eh}^2}{r_e r_{eh}}\right)\frac{\partial^2}{\partial r_e \partial r_{eh}} + \frac{2}{r_{eh}}\frac{\partial}{\partial r_{eh}} + \frac{\partial^2}{\partial r_{eh}^2} \tag{10}$$

Δ_h is obtained by interchanging the indices e by h.

The fundamental energy E_X and the corresponding envelope wave function ψ_X of the exciton, are solutions of the Schrödinger equation:

$$H_X\psi_X\left(r_e,\ r_h,\ r_{eh}\right) = E_X\psi_X(r_e,\ r_h,\ r_{eh}) \tag{11}$$

The trial wave function was chosen as:

$$\psi_X = R_e(r_e)R_h(r_h)\exp(-\alpha r_{eh}) \tag{12}$$

$\exp(-\alpha r_{eh})$ describes the Coulomb spatial correlation between the electron and the hole. α is the nonlinear variational parameter that must be determined to minimize the energy mean value. This energy is obtained by the minimization of the mean value of H_X:

$$E_X = \min\frac{<\psi_X|H_X|\psi_X>}{<\psi_X|\psi_X>} \tag{13}$$

Results and discussions

All physical parameters of materials used in the calculus are given in Table 2. The offsets of the conduction and valence band between core and shell materials are described by finite potentials: $V_e = 1.27$ eV and $V_h = 0.84$ eV for *CdSe/ZnTe* [45] and $V_e = 0.42$ eV and $V_h = 0.57$ eV for *CdSe/CdTe* [46].

From the wave functions established in different regions, we conclude that both electron and hole energies depend on the core and shell sizes and their confining potential values. Indeed, for a given shell radius (b), the electron and hole localizations depend on the core's size or the well thickness $L_W = b - a$. The resolution of the Eqs. (6) and (7) allows us to obtain the critical radii a^c_e and (a^c_h) corresponding to $E_e = V_e$ and ($E_h = V_h$) from which the electron and (hole) leave the core (shell) for a given shell size. In Fig. 2a and Fig. 2b, we plot the variation of the critical core radii a^c_e and a^c_h corresponding respectively to the switching of the electron and hole between the core and shell materials for both type II system (*CdSe/ZnTe* and *CdSe/CdTe*), as functions of the shell radius b. As we can remark, the critical radius of the electron (a^c_e) decreases as the shell radius b increases. In contrast, the critical radius of the hole (a^c_h) increases linearly as the b increases (this behavior corresponds to the type II core/shell heterostructure, and it is opposite to type I [5]). Moreover, we notice that the critical electron radius of *CdSe/ZnTe* is less than that of *CdSe/CdTe*. The critical hole radius of *CdSe/ZnTe* is more substantial than that of *CdSe/CdTe*; the difference between the calculated values of these critical radii depends on the nature of the materials and is related to the physical parameters: electron and hole masses, dielectric constants, and also to the magnitude of the band shifts.

Generally speaking, determining these limits is crucial to understanding the behavior of the correlated pair electron–hole confined in type I or type II core/shell structures where the localization of the charge carriers depends on the sizes a and b. In our case, the scenario is given in the pictorial schematic shown in Fig. 1. As we can see, for a fixed shell size (b), we can distinguish three possible configurations according to the value of the core size (a). The configuration I is obtained when $a > a^c_e$ and $a > a^c_h$, corresponding to $E_e < V_e$ and $E_h > V_h$. In this case, the electron and hole are localized in the core

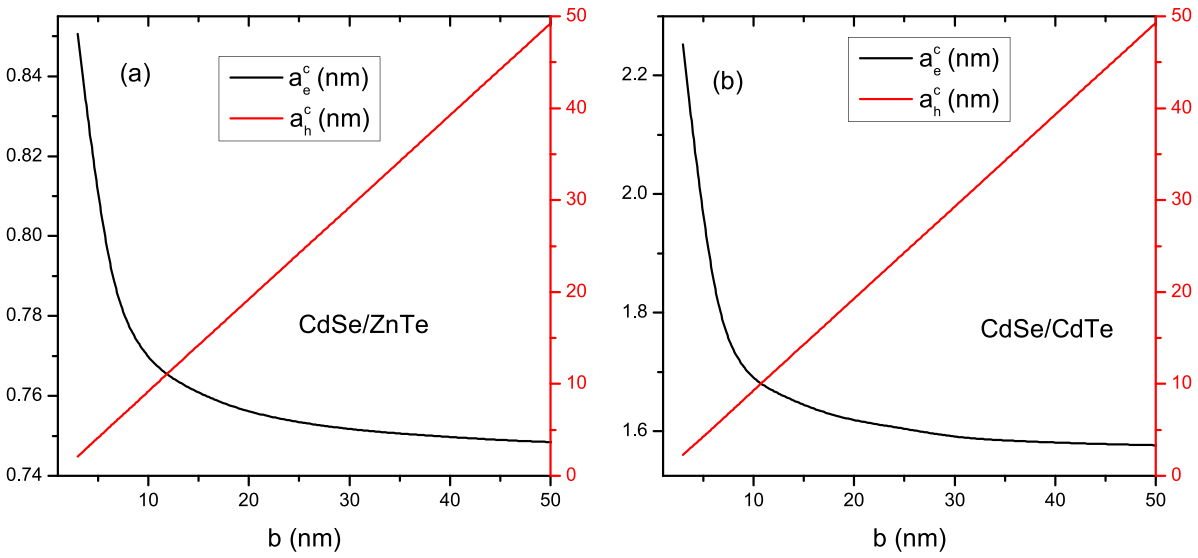

Fig. 2. Variations of the critical core radius a_e^c for the electron (black line) and a_h^c for the hole (red line) for: (a) *CdSe/ZnTe* and (b) *CdSe/CdTe*, as a function of the shell radii b. (For interpretation of the references to color in this figure legend, the reader is referred to the web version of this article.)

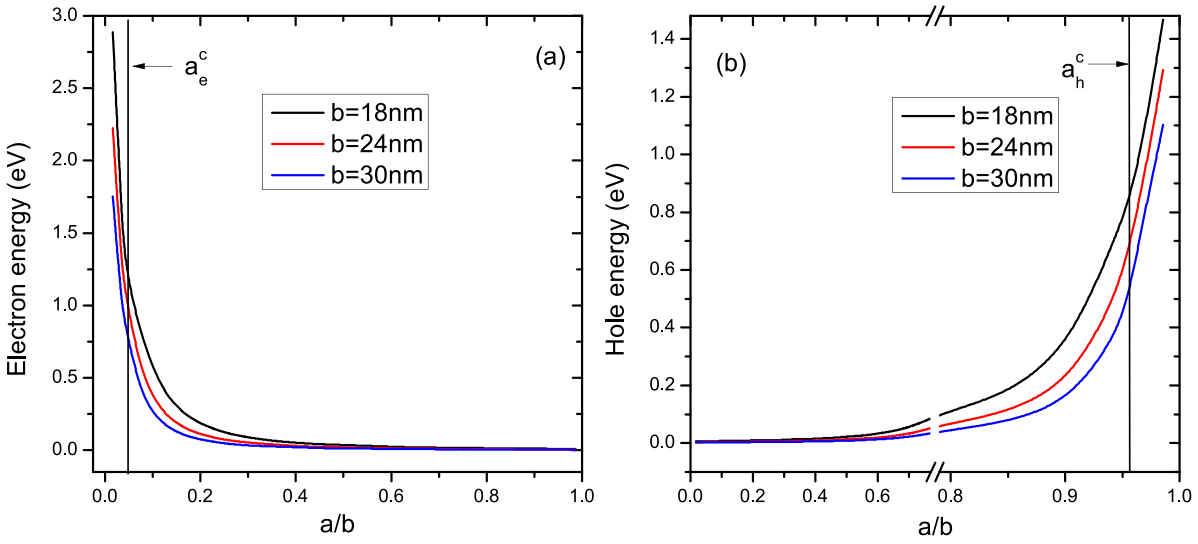

Fig. 3. Variation of the electron energy (a) the hole energy (b) of *CdSe/ZnTe* core/shell as function of the core/shell ratio a/b for $b = 18, 24$ and 30 nm.

region (Fig. 1a) then the exciton is also formed (type I exciton with Coulombic potential depending on ε_1). By reducing the core size, the hole critical radius is reached, which means that the hole escapes to the shell, whereas the electron is still in the core. This situation corresponds to the configuration II ($a > a_e^c$ and $a < a_h^c$), which corresponding to $E_e < V_e$ and $E_h < V_h$, the maximum values of electron and hole probabilities are within the core and shell, respectively (Fig. 1b), that leads to a type II exciton. In this situation, the mean value between ε_1 and ε_2 describes the potential of Coulomb. Finally, if we continue to decrease the core size, the configuration (III) characterized by: ($a < a_e^c$ and $a < a_h^c$) is obtained when $E_e > V_e$ and $E_h < V_h$. In this configuration, the electron leaves the core and joins the hole in the shell material. The maximum values of electron and hole probability densities are within the shell, and the electron–hole pair interact via a Coulomb potential depending only on ε_2 (inverted type I exciton with Coulomb potential depending on ε_2) (Fig. 1c). Our calculations show that from these critical radii values, we have a forbidden case that the electron and (hole) cannot exist within the shell and (core).

In Fig. 3a, and Fig. 4a, we plot the fundamental energy levels of the electron confined in a *CdSe/ZnTe* and *CdSe/CdTe* core/shell spherical quantum dots, respectively, as a function of the ratio a/b for different outer radius values $b = 18, 24$ and 30 nm. It is found that the electron ground state energy decreases as the outer radius b increases due to the confinement effect. We can also observe that for a fixed shell radius, the energy decreases as the a/b ratio increases from 0 to 1 due to the electron spatial confinement effect, i.e., when a tends to 0, the electron is strongly confined due to the thickness of the core which is very small in this case. In contrast, when a tends to b ($a/b \simeq 1$), the confinement of the electron becomes weak, and therefore the energy decreases. Always for a given shell radius, the electron energy comprises two regions separated by a critical radius (a_e^c); one corresponds to the unbound state when $E_e > 1.27$ eV and $E_e > 0.42$ eV, correspond to the electron confinement potential value of the*CdSe/ZnTe* and *CdSe/CdTe* respectively, in this case, the probability of the presence of the electron in the shell is more significant than in the core (Fig. 1c). A bound state corresponds to $E_e < 1.27$ eV and $E_e < 0.42$ eV, where the electron moves to the core (Fig. 1b). Turning now to the variations of the hole level energies of the core/shell *CdSe/ZnTe* and *CdSe/CdTe* QDs as a function of the ratio a/b plotted in Fig. 3b and Fig. 4b, respectively, for $b = 18, 24$ and 30 nm. As a first observation; the behavior of the

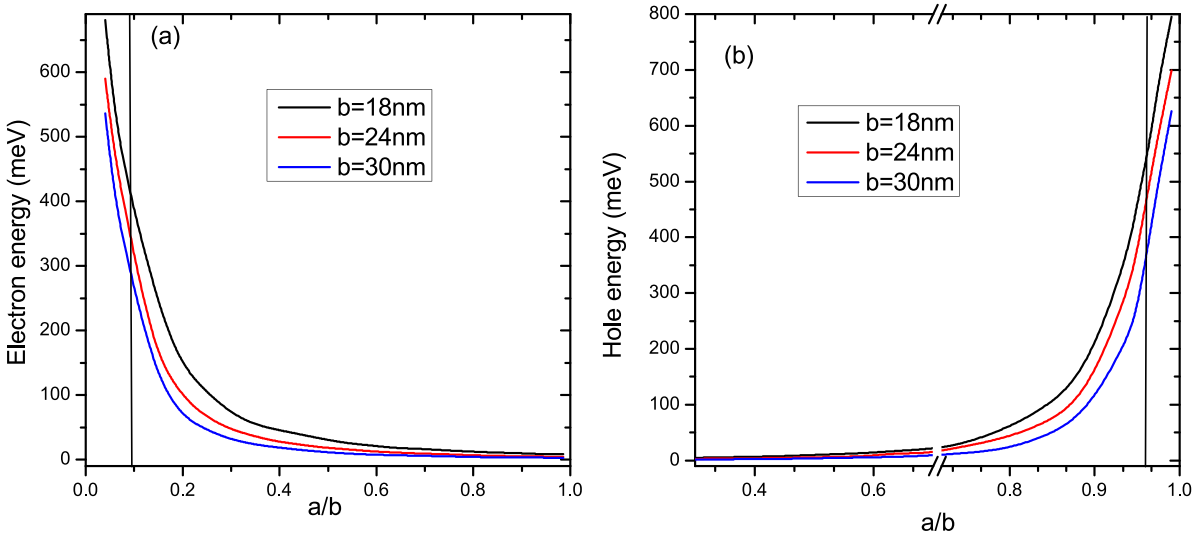

Fig. 4. Variation of the electron energy (a) and hole energy (b) of *CdSe/CdTe* core/shell as function of the core/shell ratio a/b for $b = 18, 24$ and 30 nm.

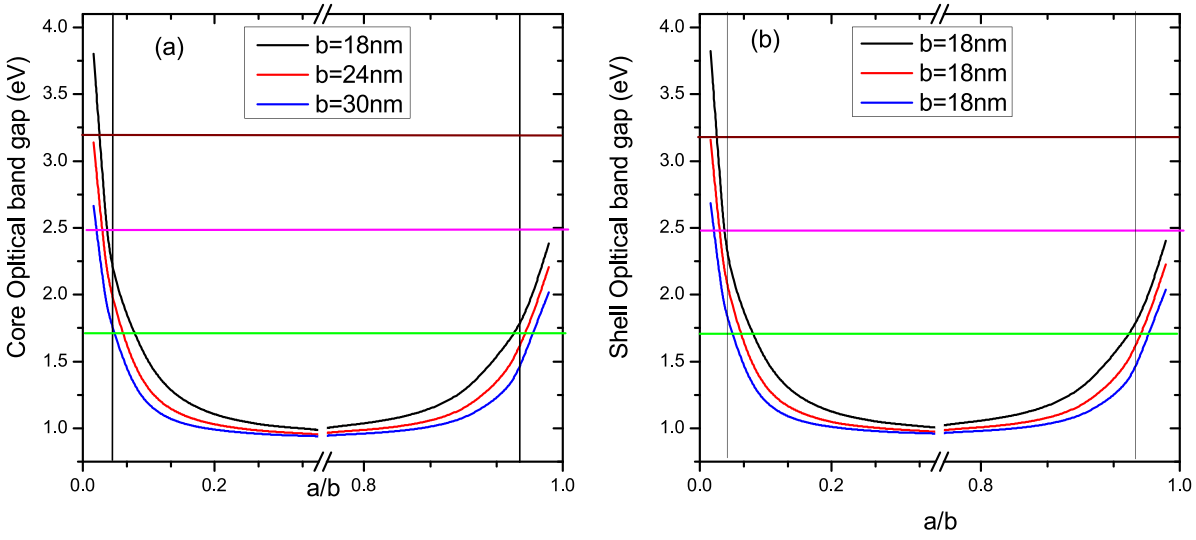

Fig. 5. Variation of the core (a) and the shell (b) optical band gap of *CdSe/ZnTe* as function of the core/shell ratio a/b for $b = 18, 24$ and 30 nm.

hole energy is opposite to that found in the case of the electrons. While increasing the core radius (a) up to a_h^c (bound state), the hole energy increases towards 0.84 *eV* and 0.57 *eV*, which correspond to the hole confinement potential in *CdSe/ZnTe* and *CdSe/CdTe*, respectively; under this situation, the hole existence probability in the core is lower than in the shell, from a_h^c to $a/b \simeq 1$, the situation changes (unbound state) and the hole existence probability in the core becomes higher than in the shell (Fig. 1a). The study shows that it is possible to switch between type I and type II electron–hole correlated pair (exciton) if the critical radius can be accurately determined when synthesizing these materials, thus widening the range of applications.

The effective optical band gap corresponding to the band alignments were determined by using the formula: $E_g^{QD} = E_e + E_h + E_g^{core} - V_h$ for the core and $E_g^{QD} = E_e + E_h + E_g^{shell} - V_e$ for the shell. Fig. 5a and Fig. 6a show the variations of the core effective gap of *CdSe/ZnTe* and *CdSe/CdTe*, respectively, as a function of the core to shell radii ratio a/b for the following shell sizes: $b = 18, 24$ and 30 nm. The green line corresponds to lower limit of visible spectrum $h\nu = 1.72$ eV (720 nm). The pink line corresponds to the middle of the visible spectrum $h\nu = 2.48$ eV (400 nm). The wine line corresponds to upper limit of the visible spectrum $h\nu = 3.18$ eV (390 nm). As we can see, the band gap transition is sensitive to the variation of the core size that controls the particles' position. For *CdSe/ZnTe* and when the ratio a/b varies from 0 to 0.5, for $b = 18$ nm, the absorption spectrum extends from near I.R through visible to ultraviolet. For a/b varies from 0.5 to 1, we have an opposite behavior compared to $0 - 0.5$ a/b variation, and the absorption spectrum extends from U.V to visible. For $b = 24$ nm and 30 nm, we remark that the absorption spectrum varies from visible to U.V, i.e., the size reduction leads to an increase in the absorption ranges. For the *CdSe/CdTe* case, we remark that when the ratio a/b varies from 0 to 0.5, the absorption spectrum varies from the lower limit of the visible to the U.V, and for a/b varies from 0.5 to 1 we have an opposite behavior compared to $0 - 0.5$ a/b variation, and the absorption spectrum, this time, extends from U.V to visible. In the shell case (Fig. 5b and Fig. 6b), we obtained the same behavior found for the core with a small change in values. Our findings are qualitatively in agreement with the experimental results found in Ref. [19,31,48–50]. As a final remark, the absorption spectrum is affected by the properties of the materials, especially the potential confinement values: large potential values enhance the absorption ranges. This result provides an accurate picture of the significant improvement in the optical gap in these structures. The optical gap diagrams are interesting for understanding optical spectra and absorption ranges. They hence help design structures for different electronic applications such as solar

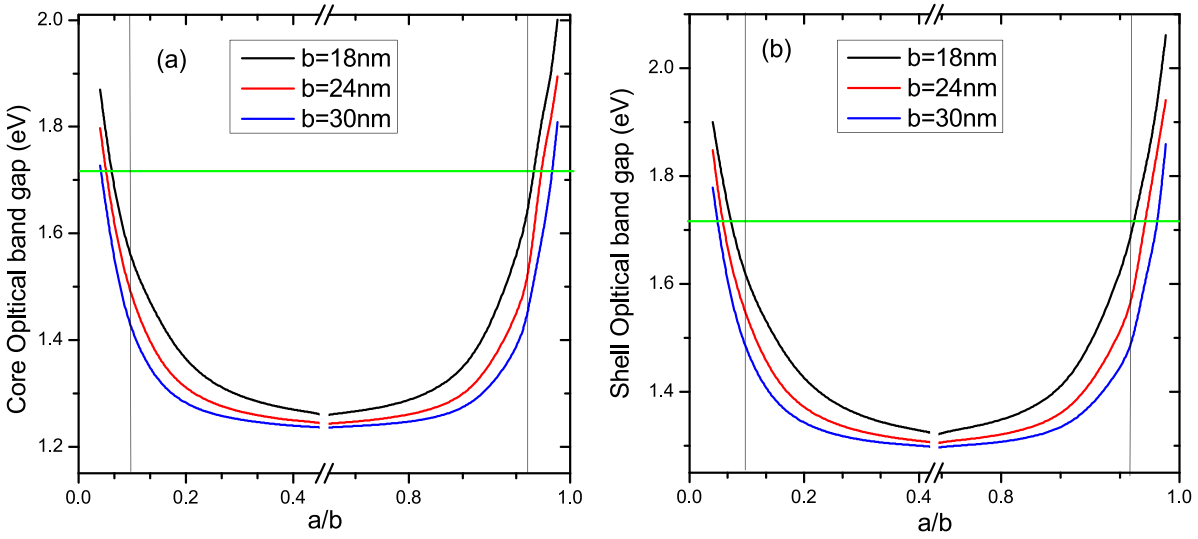

Fig. 6. Variation of the core (a) and the shell (b) optical band gap of *CdSe/CdTe* as function of the core/shell ratio a/b for $b = 18, 24$ and 30 nm.

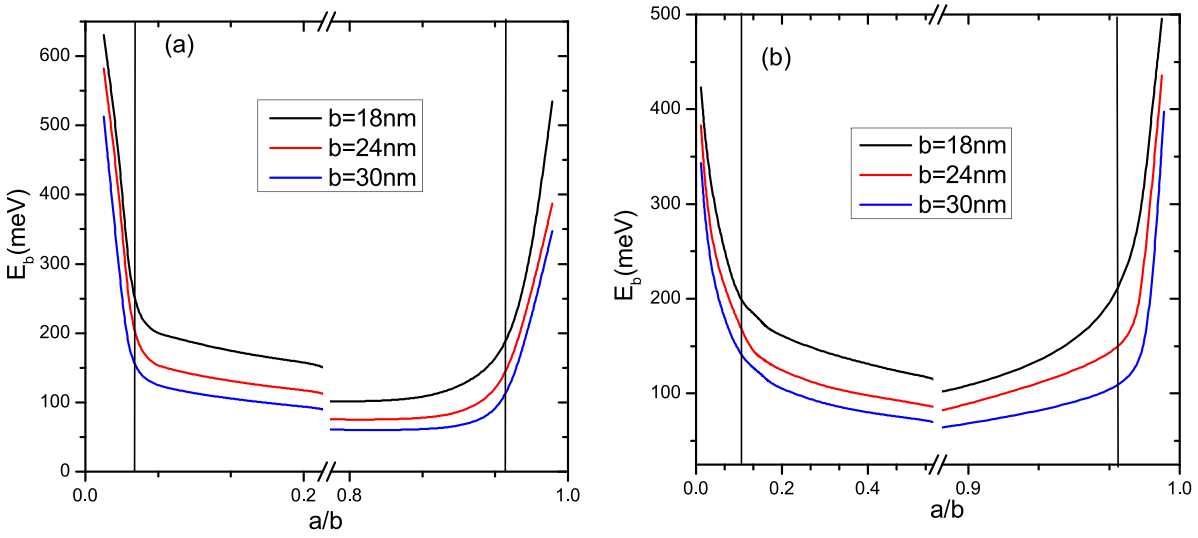

Fig. 7. Variation of the exciton binding energy of *CdSe/ZnTe* (a) and *CdSe/CdTe* (b) core/shell as function of the core/shell ratio a/b for $b = 18, 24$ and 30 nm.

cells (i.e., by using type II core/shell materials, the absorption band is expanded, and thus a more significant proportion of the incident photons can be absorbed)...; by controlling the core/shell dimensions in the two limits $a/b \simeq 0$ to a/b=0.5 and $a/b = 0.5$ to $a/b \simeq 1$.

Now we proceed to analyze the electron–hole interaction (exciton), which influences the optical spectra. For this reason, we plot in Fig. 7a and 7b, the exciton binding energy defined as: $E_b = E_e + E_h - E_T$, for *CdSe/ZnTe* and *CdSe/CdTe* type II core/shell spherical QD respectively, as a function of core to shell radii ratio a/b for $b = 18, 24$ and 30 nm. The difficulty of this problem is that for finite potentials, the wave functions of the particles are spread in the two regions (core and shell) with the possibility of passage from one side to the other by the tunnel effect; therefore, in our model, all those impacts are taken into account by investigating the three possible cases. Calculations show that the binding energy is more robust for both unbound states ($E_e > V_e$ and $E_h > V_h$), i.e., the Coulombic interaction is more important in this situation, and increases as the shell radius decrease due to the confinement effect. Also, we remark that for a given shell radius, the binding energy decreases when a/b varies from 0 to 0.8 for *CdSe/ZnTe* and from 0 to 0.83 for *CdSe/CdTe*. From $a/b = 0.8$ and 0.83, the binding energy increases and reach a maximum for $a/b \simeq 1$ i.e., the binding energy of the excitons can be controlled by adjusting the size of these nanostructures. Another remark can be extracted, the maximum of the *CdSe/ZnTe* binding energy at $a = a_e^c$ is higher than obtained for $a = a_h^c$ and is small at $a = a_e^c$ compared to $a = a_h^c$ founded in the case of *CdSe/CdTe*. This difference is attributed to the intrinsic materials' properties (confinement potentials, effective mass values, dielectric constants).

Conclusion

In the current study, we have investigated the electronic properties of uncorrelated pair electron and hole and correlated pair electron–hole (exciton) confined on a *CdSe/ZnTe* and *CdSe/CdTe* type II core/shell quantum dots taking into account the dependence of the dielectric constant. We started our work by determining the charge carriers' critical radius and ground state energies. We found that it is possible to switch between the exciton type I and type II by knowing the critical radius. After that, we analyzed the electron and hole energies, and the effective band gap. Then, we investigated the correlated electron–hole pair (exciton), which has crucial influences on the optical spectra by determining the exciton binding energy. Our findings reveal that the optical and electronic properties are strongly affected by the CSQD size. In fact, the switching between the exciton type I and type II according

to critical radii leads to a significant extension of the effective band gap that covers practically the entire visible wavelength. We expect these findings to be very useful in experimental studies concerning type II CSQD optical properties and be useful in a variety of applications such as biomedical and photovoltaic fields.

CRediT authorship contribution statement

N. Aghoutane: Conception and design of study, Acquisition of data, Analysis and/or interpretation of data, Writing – original draft. **L.M. Pérez:** Analysis and/or interpretation of data, Writing – review & editing. **D. Laroze:** Analysis and/or interpretation of data, Writing – review & editing. **M. El-Yadri:** Analysis and/or interpretation of data, Writing – original draft, Writing – review & editing. **E. Feddi:** Conception and design of study, Analysis and/or interpretation of data, Writing – original draft, Writing – review & editing.

Declaration of competing interest

The authors declare that they have no known competing financial interests or personal relationships that could have appeared to influence the work reported in this paper.

Data availability

No data was used for the research described in the article.

Acknowledgments

LMP acknowledges financial support from ANID through Convocatoria Nacional Subvención a Instalación en la Academia Convocatoria Año 2021, Grant SA77210040. DL acknowledges partial financial support from Centers of Excellence with BASAL/ANID financing, AFB180001, CEDENNA. Approval of the version of the manuscript to be published.

References

[1] Murray CB, Norris DJ, Bawendi MG. J Am Chem Soc 1993;115:8706.
[2] Yin Y, Alivisatos AP. Nature 2005;437:664.
[3] Tarucha S, Austion DG, Honda T, van der Hage RJ, Kouwenhoven LP. Phys Rev Lett 1996;77:3613–6.
[4] Banin U, Cao Yu, Katz D, Millo O. Nature 1999;400:542–4.
[5] Zouitine A, Ibral A, Assaid E, Dujardin F, Feddi E. Superlattices Microstruct 2017;109:123–33.
[6] Ibral A, Zouitine A, Assaid EM, Feddi EM, Dujardin F. Phys B 2014;449:261.
[7] Piryatinski A, Ivanov SA, Tretiak S, Klimov VI. Nano Lett 2007;7:108–15.
[8] Ivanov SA, Achermann M. ACS Nano 2010;4:5994–6000.
[9] Koç F, Sahin M. J Appl Phys 2014;115:193701.
[10] Sahin M, Koç F. Appl Phys Lett 2013;102:183103.
[11] Zhao J, Zhang J, Jiang C, Bohnenberger J, Basché T, Mews A. J Appl Phys 2004;96:3206.
[12] Vyskočil J, Hospodková A, Petřiček O, Pangrác J, Zíková M, Oswald J, et al. J Cryst Growth 2016;464:64–8.
[13] Bar M, Lehmann S, Rusu M, Grimm A, Kotschau I, Lauermann I, et al. Appl Phys Lett 2005;86:222107.
[14] Harrison P. Quantum wells, wires and dots: theoretical and computational physics. 2nd ed.. New York, USA: John Wiley; 2005.
[15] Bang J, Park J, Hwang Lee J, Won N, Nam J, Lim J, et al. Chem Mater 2010;22:233–40.
[16] Nag R, Paul S, Bera A. ChemistrySelect 2022;7:e202202802.
[17] Baylam I, Melikov R, Onal A, Oz F, Sahin M, Ow-Yang CW, et al. ACS Appl Mater Interfaces 2021;13:32022–30.
[18] Cirloganu CM, Padilha LA, Lin Q, Makarov NS, Velizhanin KA, Luo H, et al. Nature Commun 2014;5:4148.
[19] Kim S, Fisher B, Eisler HJ, Bawendi M. J Am Chem Soc 2003;125:11466–7.
[20] Balet LP, Ivanov SA, Piryatinski A, Achermann M, Klimov VI. Nano Lett 2004;4:1485–8.
[21] Oron D, Kazes M, Banin U. Phys Rev B 2007;75:035330.
[22] Klimov VI, Ivanov SA, Nanda J, Achermann M, Bezel I, McGuire JA, et al. Nature 2007;447:441–6.
[23] Osovsky R, Cheskis D, Kloper V, Sashchiuk A, Kroner M, Lifshitz E. Phys Rev Lett 2009;102:197401.
[24] Gachet D, Avidan A, Pinkas I, Oron D. Nano Lett 2010;10:164–70.
[25] Zhu H, Song N, Lian T. J Am Chem Soc 2011;133:8762–71.
[26] Barman B, Oszwałdowski R, Schweidenback L, Russ AH, Pientka JM, Tsai Y, et al. Phys Rev B 2015;92:035430.
[27] Jia Y, Chen J, Wu K, Kaledin A, Musaev DG, Xie Z, et al. Chem Sci 2016;7:4125–33.
[28] Klenovský P, Steindl P, Gefroy D. Sci Rep 2017;7:45568.
[29] Pedetti S, Ithurria S, Heuclin H, Patriarche G, Dubertret B. J Am Chem Soc 2014;136(46):16430–8.
[30] Xiao J, Zhang L, Zhou H, Shao Z, Liu J, Zhao Y, et al. ACS Appl Mater Interfaces 2020;12(28):32099–105.
[31] Ramalingam G, Ragupathi C, Rangasamy B, Colak I, Vetrivelan V, Poudineh N, et al. J Nanomater 2022;2022:1–7.
[32] Koç F, Koksal K, Sahin M. Phil Mag 2016;97:201–11.
[33] Teranishi T, Sakamoto M. J Phys Chem Lett 2013;4:2867–73.
[34] Tyrrell EJ, Smith JM. Phys Rev B 2011;84:165328.
[35] Tyrrell EJ, Tomic S. J Phys Chem C 2015;119:12720–30.
[36] Smith CT, Tyrrell EJ, Leontiadou MA, Miloszewski J, Walsh T, Cadirci M, et al. Sol Energy Mater Sol Cells 2016;158:160–7.
[37] Nandan Y, Mehata MS. Sci Rep 2019;9:2.
[38] Koç F, Kavruk AE, Sahin M. Physica E 2023;145:115479.
[39] McDonald PG, Tyrrell EJ, Shumway J, Smith JM, Galbraith I. Phys Rev B 2012;86:125310.
[40] Saravanamoorthy SN, John Peter A, Woo Lee C. Superlattices Microstruct 2017;111:1034–42.
[41] Naifar A, Zeiri N, Abdi-Ben Nasrallah S, Said M. Optik 2017;146:90–7.
[42] Chafai A, Dujardin F, Essaoudi I, Ainane A. Superlattices Microstruct 2017;101:40–8.
[43] Koç F, Sahin M. Appl Phys A 2019;125:705.
[44] Holovatsky VA, Chubrei MV, Duque CA. Thin Solid Films 2022;747:139142.
[45] Davies JH. The physics of low-dimensional semiconductors : An introduction. Cambridge University Press; 2005.
[46] David Kumar MM, Devadason S. Appl Nanosci 2013;3:453–9.
[47] Borisenko VE, Ossicini S. What is what in the nanoworld. Wiley-VCH Verlag & Co. KGaA; 2012.
[48] Kaniyankandy S, Rawalekar S, Verma S, Ghosh HN. J Phys Chem C 2011;115:1428–35.
[49] Liu Y, Zhang C, Zhang H, Wang R, Hua Z, Wang X, et al. Adv Mater 2013;25:4397–402.
[50] Leontiadou MA, Tyrrell EJ, Smith CT, Espinobarro-Velazquez D, Page R, O'Brien P, et al. Sol Energy Mater Sol Cells 2017;159:657–63.